Journal of Alloys and Compounds 1020 (2025) 179211

Contents lists available at ScienceDirect

Journal of Alloys and Compounds

journal homepage: www.elsevier.com/locate/jalcom

Growth, spectroscopy and laser operation of disordered Tm,Ho:NaGd$(MoO_4)_2$ crystal

Ghassen Zin Elabedine [a], Zhongben Pan [b], Pavel Loiko [c], Hongwei Chu [b], Dechun Li [b], Kirill Eremeev [c], Kirill Subbotin [d], Sergei Pavlov [d], Patrice Camy [c], Alain Braud [c], Sami Slimi [a], Rosa Maria Solé [a], Magdalena Aguiló [a], Francesc Díaz [a], Weidong Chen [e,f], Uwe Griebner [e], Valentin Petrov [e], Xavier Mateos [a,*,1]

[a] Universitat Rovira i Virgili (URV), Física i Cristal·lografia de Materials (FiCMA), Tarragona 43007, Spain
[b] School of Information Science and Engineering, Shandong University, Qingdao 266237, China
[c] Centre de Recherche sur les Ions, les Matériaux et la Photonique (CIMAP), UMR 6252 CEA-CNRS-ENSICAEN, Université de Caen Normandie, 6 Boulevard Maréchal Juin, Caen Cedex 4 14050, France
[d] Prokhorov General Physics Institute, Russian Academy of Sciences, 38 Vavilova St, Moscow 119991, Russia
[e] Max Born Institute for Nonlinear Optics and Short Pulse Spectroscopy, Max-Born-Str. 2a, Berlin 12489, Germany
[f] State Key Laboratory of Functional Crystals and Devices, Fujian Institute of Research on the Structure of Matter, Chinese Academy of Sciences, 350002 Fuzhou, China

ARTICLE INFO

Keywords:
Double molybdates
Holmium doping
Optical spectroscopy
Luminescence
Energy transfer
2-micron solid-state lasers

ABSTRACT

We report on the growth, structure refinement, Raman and optical spectroscopy, and first laser operation of Tm^{3+},Ho^{3+}-codoped disordered sodium gadolinium double molybdate. A single crystal of 5.55 at% Tm, 0.43 at% Ho:NaGd$(MoO_4)_2$ was grown by the Czochralski method in argon atmosphere. Its structure was refined by the Rietveld method (sp. gr. $I4_1/a$, lattice constants: $a = 5.237(5)$ Å and $c = 11.443(6)$ Å). The Raman spectroscopy revealed a dominant high-frequency mode at 883 cm^{-1} due to symmetric stretching vibrations of the $[MoO_4]^{2-}$ groups. The stimulated-emission cross-section for the $^5I_7 \rightarrow {}^5I_8$ transition of the Ho^{3+} ion is 1.84×10^{-20} cm^2 at 2043 nm for π-polarization and the emission bandwidth is as broad as 66 nm for σ-polarized light. The parameters of the $Tm^{3+} \rightarrow Ho^{3+}$ energy transfer were quantified revealing a thermal equilibrium decay time of the $^3F_4(Tm^{3+})$ and $^5I_7(Ho^{3+})$ multiplets of 3.8 ms. The continuous-wave Tm,Ho-laser generated 548 mW at 2045 – 2055 nm with a slope efficiency of 32.4 %, a laser threshold of 98 mW and a liner polarization (π). Due to its inhomogeneously broadened emission bands, the Tm,Ho:NaGd$(MoO_4)_2$ crystal is promising for mode-locked lasers.

1. Introduction

Current trends in laser engineering include the research on ultrafast sources. The development of laser oscillators capable of generating ultrashort (few optical cycle) pulses is strongly dependent on material engineering capable of tailoring the gain bandwidth of active media [1]. Broad, smooth and nearly structureless gain profiles are desirable. They are readily achieved in rare-earth doped glasses [2]. However, glassy gain media suffer from poor thermal properties. An alternative approach consists of utilizing crystalline materials with structure disorder. Such disordered crystals, e.g., garnets or aluminates, have recently gained a lot of attention for the generation of ultrashort pulses from mode-locked lasers [3,4].The structure disorder can induce a significant inhomogeneous spectral line broadening leading to a "glassy-like" spectroscopic behavior at higher thermal conductivity [5].

Rare-earth-doped tetragonal scheelite-type double tungstate and double molybdate crystals with a common general formula $MRE(TO_4)_2$, where M represents an alkali metal (Li or Na), RE denotes a rare-earth (La, Gd, Y, Lu) or Bi, and T is W or Mo, respectively, are known for applications as laser gain media, including ultrafast lasers [6–9]. They adopt a centrosymmetric space group $I4_1/a$ or lower space groups ($I4$, $I/4$) depending on the particular character of a nearly random distribution of M^+ and RE^{3+} cations over two non-equivalent lattice sites (Wyckoff: 2*b* and 2*d*) with S_4 symmetry [6,10–12]. The local disorder is

* Corresponding author.
E-mail address: xavier.mateos@urv.cat (X. Mateos).
[1] Serra Húnter Fellow, Spain

https://doi.org/10.1016/j.jallcom.2025.179211
Received 28 September 2024; Received in revised form 30 January 2025; Accepted 13 February 2025
Available online 14 February 2025

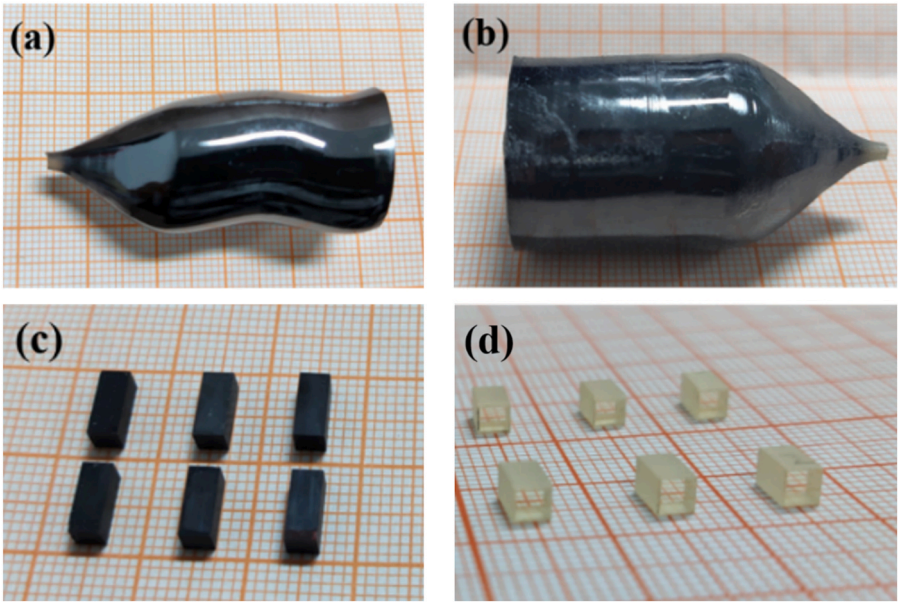

Fig. 1. Photographs of the as-grown Tm,Ho:NaGd$(MoO_4)_2$ crystals: growth (a) using a Pt wire; (b) using a single-crystalline seed oriented along the [001] axis; (c,d) parallepipedic crystal samples: (c) before annealing, (d) after annealing and polishing.

explained by the short-range M^+/RE^{3+} distribution, i.e., the second coordination sphere, around each of the 2*b* and 2*d* sites. In this way, multiple cationic environments around the dopant ions replacing for the host-forming RE^{3+} cations can be expected, adopting symmetries from S_4 (when all the neighbor cations are the same) to C_2 or even C_1 (for "mixed" environments). This leads to a strong spectral line broadening even at cryogenic temperatures. The highest degree of disorder is associated with equal occupancy factors for both M^+ and RE^{3+} cations.

The structure disorder of MRE$(TO_4)_2$ crystals is manifested in broad and nearly structureless absorption and emission bands for polarized light (these crystals are optically uniaxial [13]). Other advantages of these compounds include relatively easy doping due to a substitutional rare-earth site, and a weak concentration quenching of luminescence. The considered crystals are also known as efficient Raman frequency shifters [14]. The MRE$(TO_4)_2$ compounds can be grown by the Czochralski (Cz) or Top-Seeded solution Growth methods. Despite their relatively low thermal conductivity ($\kappa_a = 1.10$ and $\kappa_c = 1.24$ $Wm^{-1}K^{-1}$ for NaGd$(WO_4)_2$ [15]), owing to their overall thermo-optic behavior [16], rare-earth doped MRE$(TO_4)_2$ crystals outperform glasses.

For solid-state laser development targeting the eye-safe spectral range of 2 μm, Thulium (Tm^{3+}) and Holmium (Ho^{3+}) dopant ions are usually considered. Their emission originates from the spectrally overlapping $^3F_4 \rightarrow {}^3H_6$ and $^5I_7 \rightarrow {}^5I_8$ transitions, respectively. The Ho^{3+} ion emits above 2 μm, in a spectral range free of water absorption lines in the air, which represent a limiting factor for femtosecond pulse generation. To excite Ho^{3+} ions, often, the Tm^{3+}, Ho^{3+} codoping scheme is employed [17–19], as Tm^{3+} ions act as donors (D) by absorbing the pump radiation around 0.8 μm and transferring it non-radiatively to Ho^{3+} ones (acceptors, A), $^3F_4(Tm^{3+}) \rightarrow {}^5I_7(Ho^{3+})$. Apart from the simplified pump configuration which can rely on commercial and power scalable AlGaAs laser diodes, the codoped materials benefit from combined gain bandwidths of the two ions, contributing to the pulse shortening in mode-locked lasers [20,21]. Recently, sub-100 fs lasers emitting around 2 μm have been demonstrated employing Tm^{3+}, Ho^{3+}-codoped disordered gain media [3,4,20,21]. Ultrafast 2-μm lasers find their application niches in frequency down-conversion towards the mid-infrared spectral range, THz and high-harmonic generation and time-resolved pump-probe spectroscopy [22]. Tunable 2-μm lasers based on Thulium and/or Holmium ion emission are in general interesting not only for spectroscopic research, but also important for applications in medicine (laser surgery), environmental monitoring (*e.g.*, H_2O, CO_2) and material processing (welding and cutting of plastics).

MRE$(TO_4)_2$ type crystals have been studied for single Tm^{3+} [23–26] and Ho^{3+} [27,28] doping, as well as Tm^{3+},Ho^{3+} codoping [7,29,30], regarding their spectroscopic properties and laser operation. Han *et al.* reported on continuous-wave and tunable operation of Tm^{3+}, Ho^{3+}-codoped NaY$(WO_4)_2$ and NaLu$(WO_4)_2$ crystals: with the former material, an output power of 265 mW at 2.05 μm was extracted corresponding to a slope efficiency of 43 % and a broadband wavelength tuning across 1825 – 2080 nm was obtained [31]. Tang *et al.* explored the Tm,Ho:LiGd$(MoO_4)_2$ crystal delivering only 25 mW at 2.05 μm with a slope efficiency of 20 % [30].

In contrast to potassium containing double tungstate and molybdate compounds, which undergo polymorphic transformations upon cooling after growth, for Na-based tungstates and molybdates, the tetragonal phase is stable in the whole temperature range from 300 K to the melting point, allowing for the Czochralski growth (except for NaLu$(MoO_4)_2$ and NaLu$(WO_4)_2$, which melt incongruently). Tetragonal double molybdates offer better spectroscopic properties as compared to their tungstate counterparts, namely, higher absorption and emission cross-sections [8]. Among them, sodium gadolinium double molybdate, NaGd$(MoO_4)_2$ (space group: $I4_1/a$, abbreviated: NGM), attracts a lot of attention. The spectroscopy and (in certain cases) laser operation of NaGd$(MoO_4)_2$ doped with Nd^{3+} [32], Yb^{3+} [33], Tm^{3+} [6,23,34], and Ho^{3+} [35,36] ions were reported. The authors of [37] performed a comprehensive study of spectroscopic characteristics of a series of Tm^{3+}-doped $NaLa_{1-x}Gd_x(MoO_4)_2$ mixed crystals for the entire range of $x = 0$ – 1 including the end-member of this series, the Tm:NaGd$(MoO_4)_2$ crystal. Han *et al.* presented a Tm:NaGd$(MoO_4)_2$ laser delivering 850 mW at 1.90 μm with a slope efficiency of 45 % and a laser threshold of 180 mW, as well as a wavelength tuning from 1875 to 1975 nm [24]. Bol'shchikov *et al.* reported on diode-pumped laser operation of a "mixed" Tm:$NaLa_{1/3}Gd_{2/3}(MoO_4)_2$ crystal delivering 210 mW at 1.91 μm with a slope efficiency of 27 % and a laser threshold of 550 mW, as well as a wavelength tuning from 1860 to 1955 nm, with the beam quality being close to the diffraction-limited one [38]. Wang *et al.* studied the thermal and unpolarized spectroscopic properties of a Tm,Ho:NaGd$(MoO_4)_2$ crystal [29].

In the present work, we report on the Cz growth, structure refinement, polarized Raman and optical spectroscopy and first continuous-

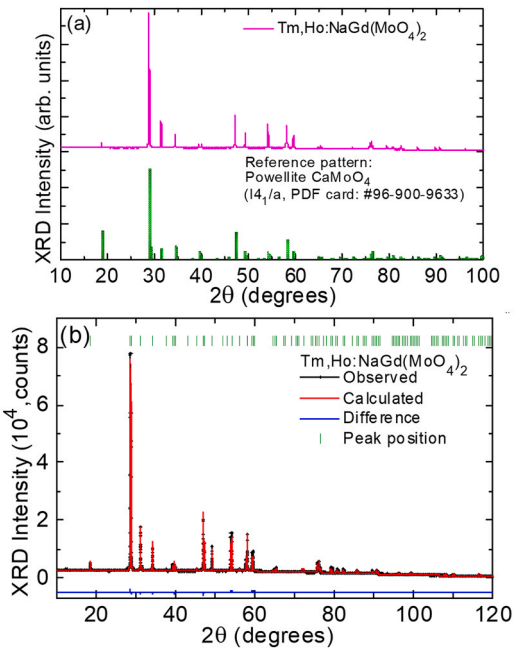

Fig. 2. (a) X-ray powder diffraction (XRD) pattern of Tm,Ho:$NaGd(MoO_4)_2$ crystal (magenta) and the reference pattern of powellite $CaMoO_4$ adopting the sp. gr. $I4_1/a$ (green bars), PDF card #96–900–9633, COD database; (b) Rietveld refinement: observed (black), calculated (red), and residual (blue) patterns, green dashes - Bragg reflections.

wave laser operation of Tm^{3+},Ho^{3+}-codoped disordered $NaGd(MoO_4)_2$ crystals with the goal of developing novel broadly emitting materials for ultrafast lasers around 2 μm.

2. Crystal growth

A $NaGd(MoO_4)_2$ single crystal co-doped with 5 at% Tm^{3+} and 0.5 at % Ho^{3+} (in the melt) was grown by the standard Cz method in argon atmosphere using an iridium crucible. The starting materials were $NaCO_3$ (purity: 4 N), Gd_2O_3, Tm_2O_3, Ho_2O_3, and Mo_2O_3 (5 N). They were accurately weighed according to the chemical formula $NaGd_{0.945}Tm_{0.05}Ho_{0.005}(MoO_4)_2$. To counteract the volatilization of Mo_2O_3 during the synthesis of the polycrystalline material and the crystal growth, an excess of 2.0 wt% Mo_2O_3 was added. The equation of the solid-state chemical reaction is expressed as follows:

$$Na_2CO_3 + 0.945Gd_2O_3 + 0.05Tm_2O_3 + 0.005Ho_2O_3 + 4Mo_2O_3 \rightarrow 2NaGd_{0.945}Tm_{0.05}Ho_{0.005}(MoO_4)_2 + CO_2\uparrow.$$

The mixture was subsequently put together, ground, and heated at 650 ℃ for 10 h (h) in a platinum crucible to decompose Na_2CO_3. After cooling to room temperature (RT, 293 K), the mixture was pressed into pellets and reheated at 950 ℃ for 15 h to form the tetragonal molybdate phase via solid-state reaction.

The synthesized polycrystalline material was placed in an iridium crucible and melted using an intermediate-frequency heater. Typically, to eliminate bubbles from the melt and prevent the formation of polycrystals during growth, the melt was maintained at a temperature 30–50 ℃ above the melting point for about 2–3 h before cooling it to the melting point. During the crystal growth, the pulling rate varied from 0.5 to 1.0 mm/h, and the crystal rotation speed was 8–15 revolutions per minute (rpm). An automated system was used to regulate the boule diameter. Following completion of the growth, the crystal was cooled to RT at a stepped rate of 15–25 ℃/h.

Initially, a Pt wire was used as a seed for the crystal growth, resulting in a crystal boule with a nearly black coloration and spiral growth, Fig. 1 (a). Subsequently, a seed oriented along the crystallographic [001] axis was cut from this first crystal, yielding a crystal boule with a larger size and minimal spiral growth, Fig. 1(b). The observed spiral growth could be attributed to poor heat dissipation due to the low thermal conductivity of this double molybdate. In addition, non-symmetrical breakdown of the facet formation might contribute to this phenomenon. Both crystal boules were nearly black, primarily due to the presence of color centers associated with oxygen vacancies but annealing in air significantly improved their transparency. Small crystal samples were cut from the as-grown crystal boule, Fig. 1(c), and after annealing at 900 ℃ for 72 h in air, the coloration was almost completely removed, resulting in nearly colorless samples, Fig. 1(d). When observing the internal quality of the polished samples, Fig. 1(d), with a He-Ne laser, no scattering centers were found, indicating an excellent optical quality.

Using X-ray fluorescence, the actual Tm^{3+} and Ho^{3+} doping levels in the $NaGd(MoO_4)_2$ crystal were measured to be 5.55 at% (ion density: $N_{Tm} = 3.54 \times 10^{20}$ at/cm^3) and 0.43 at% ($N_{Ho} = 2.74 \times 10^{19}$ at/cm^3), respectively, and the segregation coefficients of the dopant ions were evaluated, $K_{RE} = C_{crystal}/C_{melt}$, yielding $K_{Tm} = 1.11$ and $K_{Ho} = 0.86$. The obtained value of K_{Tm} appeared to be much higher than that determined earlier, $K_{Tm} = 0.54$ [37].

3. Experimental

The X-ray powder diffraction (XRD) pattern was measured using a Bruker D2 Phaser diffractometer for diffraction angles 2θ in the range of 5–120° with a step of 0.02° using Cu Kα1 radiation.

The polarized Raman spectra were measured for an ***a***-cut Tm,Ho:$NaGd(MoO_4)_2$ crystal using a Renishaw inVia confocal Raman microscope equipped with a × 50 Leica objective, an Ar^+ ion laser (λ = 488 nm), and a set of polarizing optics. Porto's notations were used, ***a*** (*ij*)$\bar{\boldsymbol{a}}$, where "***a***" and "$\bar{\boldsymbol{a}}$" represent the propagation directions of the incident and scattered light, respectively, and "*i*" and "*j*" signify the corresponding polarization states (π or σ).

The polarized absorption spectra were measured using a Varian CARY 5000 spectrophotometer and a calcite Glan-Taylor polarizer

The luminescence spectra were measured using an optical spectrum analyzer (OSA, Yokogawa AQ6376) purged by N_2 gas to mitigate the influence of the structured water vapor absorption in the air around 2 μm. The emission was collected using a CaF_2 lens and a large mode area ZrF_4 fiber. A metal-grid polarizer was also employed. The excitation was provided by a Ti:Sapphire laser at 795 nm (excitation to the $^3H_4$ multiplet of Tm^{3+}).

The luminescence decay was studied employing a nanosecond optical parametric oscillator (Horizon, Continuum), a 1/4 m monochromator (Oriel 77200), an InGaAs detector, and an 8 GHz digital oscilloscope (DSA70804B, Tektronix). To mitigate the impact of radiation trapping, the samples were ground into fine powders.

The low-temperature measurements were enabled by a cryostat (Oxford Instruments, model SU 12) equipped with helium-gas close-cycle flow.

4. Crystal structure and Raman spectra

4.1. X-ray diffraction

The crystal structure of teteragonal scheelite-type double tungstate and double molybdates was a subject of detailed investigations by multiple groups, see for example Cano-Torres *et al.* [6]. We employed the powder XRD analysis and the Rietveld method for refining the unit-cell parameters and atomic coordinates of the Tm^{3+},Ho^{3+}-codoped $NaGd(MoO_4)_2$ crystal. All the observed diffraction peaks demonstrated a close correspondence with the reference powellite phase, $CaMoO_4$ (tetragonal class, space group $I4_1/a$ – $C_{4\,h}^6$, No. 88), the Crystallography Open Database (COD) card #96–900–9633, Fig. 2(a). The lack of diffraction peaks related to impurity and secondary phases indicated a single-phase nature of the grown crystal.

Table 1
Rietveld refinement parameters for Tm,Ho:NaGd$(MoO_4)_2$.

Data	Tm,Ho:NaGd$(MoO_4)_2$
Crystal System	Tetragonal
Space group (Z)	$I4_1/a$ (Z = 2)
Laue class	$4/m$
Lattice constant $a = b$, c (Å)	5.237(5), 11.443(6)
$\alpha = \beta = \gamma$ (deg.)	90
Volume (Å^3)	313.9(1)
Calculated density (g/cm^3)	5.519
2θ range (deg.)	5–120
2θ step (deg.)	0.02
Radiation	Cu-Kα1 (λ = 1.5418 Å)
No. of reflections	238
Refinement software	Match! 3.0
Reliability factors	R_p = 2.48, R_{wp}= 3.78, R_{exp}= 2.16 and χ^2 = 3.07

Table 2
Fractional atomic coordinates (x, y, z), site occupancies (O.F.), Wyckoff positions and isotropic displacement parameters (B_{iso}) for Tm,Ho:NaGd$(MoO_4)_2$ crystal.

Atoms	Wyckoff	*x*	*y*	*z*	O.F.	B_{iso} (Å^2)
Na	4*b*	0	1/4	0.6250(0)	0.500	2.099(1)
Gd| Tm| Ho	4*b*	0	1/4	0.6250(0)	0.470| 0.028| 0.002	2.099(1)
Mo	4*a*	0	1/4	0.1250(0)	1	3.220(1)
O	16*f*	0.2572(6)	0.0933 (9)	0.0460(2)	1	1.600 (0)

Table 3
Selected interatomic distances in the Tm,Ho:NaGd$(MoO_4)_2$ crystal.

Atoms	Distances (Å)
Mo– O	1.8182(7) × 4
Na|RE– O	2.3807(5) × 4 2.4734(3) × 4
Na|RE– Na|RE	3.8784(9) × 4 #1 5.2375(3) × 4 #2

The crystal structure refinement was performed by the Rietveld method using the Match! 3.0 software. We used the starting structural model and the crystallographic data reported by Cheng *et al.* for LiLu$(MoO_4)_2$ [39]. Chimitova *et al.* have presented a systematic review of MRE$(MoO_4)_2$ double molybdates and divided them into several groups based on the ratio of the ionic radii of the M^+ and RE^{3+} cations ($t = R_M/R_{RE}$) [40]. The MRE$(MoO_4)_2$ compounds exhibiting *t* values falling within the 0.805–1.341 range typically adopt a tetragonal unit-cell with either $I4_1/a$ or I-4 symmetry. The *t* ratio is the key structural parameter of all double molybdates as the structure is weakly dependent on the volume of the unit-cell and the nature of the A^+ and Ln^{3+} cations. The NaGd$(MoO_4)_2$ crystal is expected to possess the $I4_1/a$ space group, owing to its calculated *t* value of 1.121 (R_{Na} = 1.18 Å and R_{Gd} = 1.053 Å for VIII-fold oxygen coordination). Considering the ionic radii and the valence state, the incorporation of $Tm^{3+}$and Ho^{3+} dopant ions into the crystal lattice of NaGd$(MoO_4)_2$ involves occupation of Gd^{3+} sites. The corresponding site occupancies were taken according to the X-ray fluorescence data. The results of the Rietveld refinement are presented in Fig. 2(b) depicting the measured, calculated and residual profiles, as well as the Bragg reflections. The *R*-factors were R_p = 2.48 %, R_{wp} = 3.78 %, and R_{exp} = 2.16 %, leading to a reasonable χ-squared value of χ^2 = 3.07, indicating convergence of the fit (Table 1).

Upon refinement, it could be confirmed that Tm,Ho:NaGd$(MoO_4)_2$ adopts the tetragonal $CaMoO_4$-type structure. The lattice parameters are $a = b$ = 5.237(5) Å and c = 11.443(6) Å, $\alpha = \beta = \gamma = 90°$ (number of the formula units per unit-cell: $Z = 2$). The unit-cell volume V is 313.9(1) Å^3, yielding a calculated density ρ_{calc} of 5.519 g/cm^3. The Tm^{3+} and Ho^{3+} doping does not change the structure of the host matrix. For undoped NaGd$(MoO_4)_2$, $a = b$ = 5.2325(2) Å, c = 11.4405(6) Å, and V = 313.23(3) Å^3 [41].

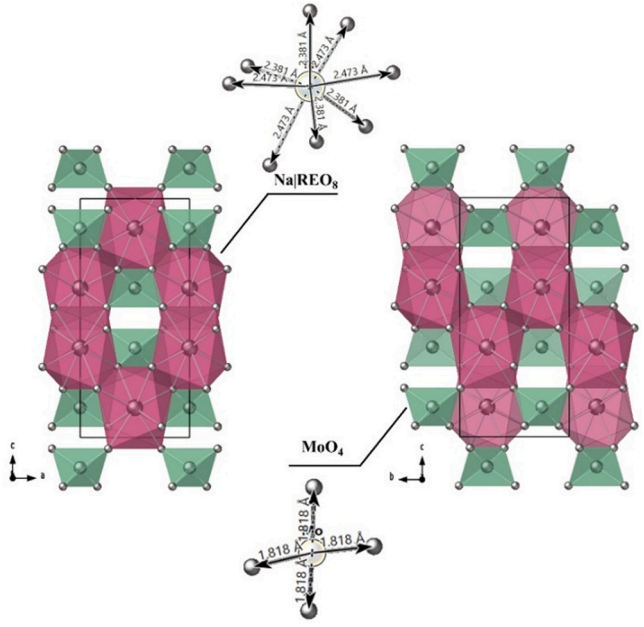

Fig. 3. The crystal structure of Tm,Ho:NaGd$(MoO_4)_2$ in projection to the **a-c** (left) and **b-c** (right) crystallographic planes. The metal-to-oxygen interatomic distances are shown.

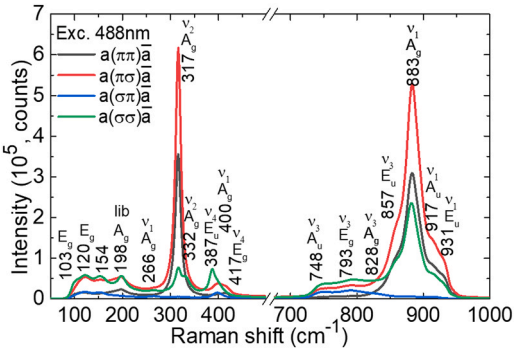

Fig. 4. Polarized Raman spectra of the Tm,Ho:NaGd$(MoO_4)_2$ crystal for the **a** (ij)$\bar{a}$ geometries (i, j = π or σ). The numbers indicate the Raman band frequencies in cm^{-1}. λ_{exc} = 488 nm.

Table 2 lists the fractional atomic coordinates, site occupancy factors (O.F.), and isotropic displacement parameters (B_{iso}) obtained during the Rietveld refinement. Selected interatomic distances are shown in Table 3, and a fragment of the crystal structure in projection to the ***a-c*** and ***b-c*** crystallographic planes is provided in Fig. 3. Mo atoms reside in 4*a* Wyckoff sites, and they are IV-fold oxygen coordinated forming tetrahedrons (the Mo – O interatomic distances are 1.8182(7) Å). Both Na^+ and rare-earth (Gd^{3+}, Tm^{3+}, Ho^{3+}) ions are statistically distributed over 4*b* sites with VIII-fold coordination by oxygen in a ratio of 1:1. There are two distinct Na|RE – O distances, namely 2.3807(5) Å (×4) and 2.4734 (3) Å (×4), resulting in a snub disphenoid polyhedron with deltahedral coordination (8 vertices, 12 faces, and 18 edges). The [Na|REO_8] dodecahedrons are connected to the [MoO_4] tetrahedrons via bridging oxygen atoms. These Na|RE–O–Mo bridges are analogous to those encountered in scheelite structures. The shortest observed Gd - Gd

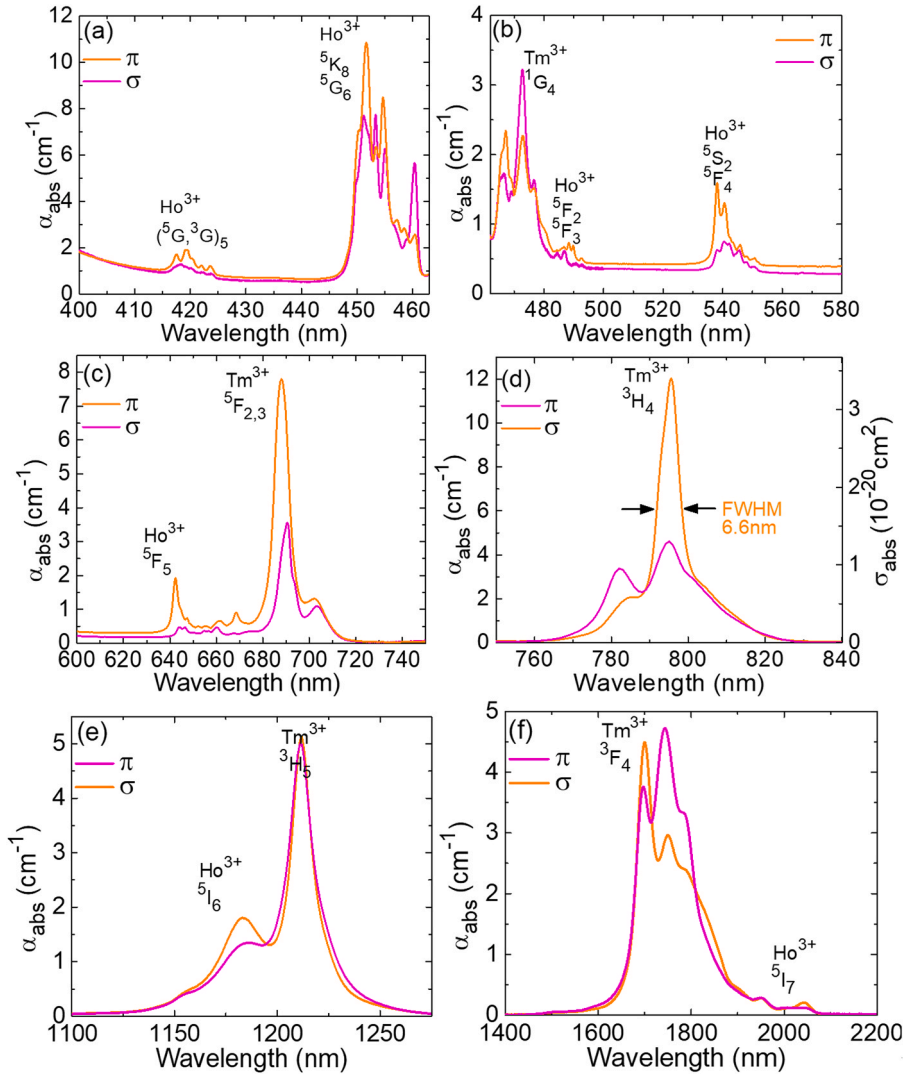

Fig. 5. (a-f) Polarized absorption spectra of the 5.55 at% Tm, 0.43 at% Ho:$NaGd(MoO_4)_2$ crystal, light polarizations: π and σ.

interatomic distance is along the vector $[u,v,w] = [1/2,0,1/4]$, measuring 3.8784(9) Å. Notably, this distance extends to 5.2375(3) Å along the ***a***-axis in the ***a***-***c*** plane.

4.2. Raman spectroscopy

The polarized Raman spectra of the ***a***-cut Tm,Ho:$NaGd(MoO_4)_2$ crystal are shown in Fig. 4. The spectra consist of broadened, mutually overlapping bands. This is a typical situation for structurally disordered crystals. The spectra can be divided into two frequency regions: a low frequency region at 103–417 cm^{-1}, where the modes are due to the "skeletal" (external) motions, and a high-frequency region, between 748 and 931 cm^{-1}, for which the modes originate from the internal vibrations of the $[MoO_4]^{2-}$ groups. No Raman bands between these two ranges are observed due to the lack of double oxygen bridge vibrations in contrast to monoclinic double tungstates and molybdates. The strongest high-frequency Raman peak at 883 cm^{-1} corresponds to symmetric stretching vibrations of the $[MoO_4]^{2-}$ anion, the $\nu_1(A_g)$ mode according to the scheelite $I4_1/a$ symmetry [42].

5. Optical spectroscopy

The tetragonal $NaGd(MoO_4)_2$ crystal is optically uniaxial, and its optical axis is parallel to the crystallographic ***c***-axis. The two principal light polarizations are $\boldsymbol{E} \parallel \boldsymbol{c}$ (π) and $\boldsymbol{E} \perp \boldsymbol{c}$ (σ), and the corresponding refractive indices are n_e and n_o. At ~2 μm, their values are $n_e = 1.967$ and $n_o = 1.960$ (indicating an optically positive crystal). An ***a***-cut crystal was used for the spectroscopic measurements giving access to both principal light polarizations.

5.1. Optical absorption

The polarized absorption spectra are shown in Fig. 5(a–f). They contain the absorption bands of both Tm^{3+} and Ho^{3+} ions. For Tm^{3+} dopant ions, the transitions in absorption originate from the $^3H_6$ ground state and terminate at various excited states spanning from $^3F_4$ to $^1G_4$. For Ho^{3+} ions, the ground state is $^5I_8$ and the observed transitions in absorption terminate at the excited states from $^5I_7$ to $(^5G,^3G)_5$. The multiplet assignment follows the work of Carnall et al. [43]. The UV absorption edge for the studied crystal is at 387 nm (optical bandgap: 3.20 eV). The bandgap of an isostructural $NaY(MoO_4)_2$ crystal (undoped) E_g is 3.28 eV (determined from the absorption edge) [44]. Nearly the same UV absorption edge had been observed earlier for scheelite-like $NaLa(MoO_4)_2$ crystal [45]. However, when the same crystal was grown using a starting reagent of MoO_3 which passed through a special procedure of very deep purification, the UV absorption edge of the crystal was further blue shifted by ~15 nm. Therefore, the optical absorption in the range of at least 370–390 nm is caused by accidental impurities.

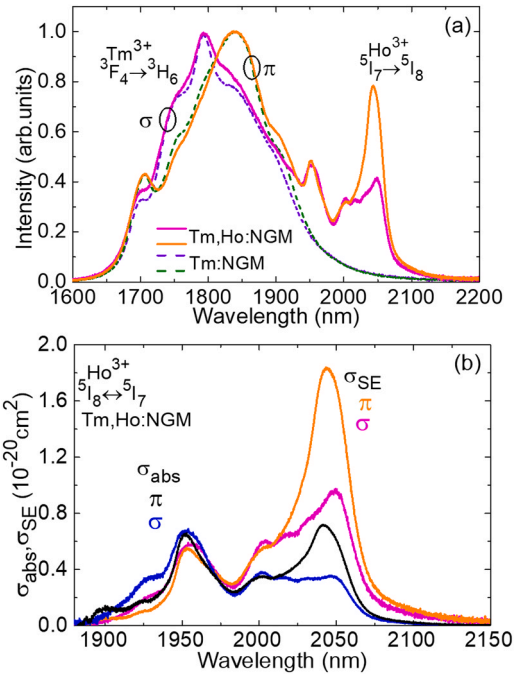

Fig. 6. Emission properties of Tm^{3+} and Ho^{3+} ions in the $NaGd(MoO_4)_2$ crystal: (a) luminescence spectra of a codoped crystal (solid curves), the spectra for a singly Tm^{3+}-doped one (dashed curves) are given for comparison; (b) absorption, σ_{abs}, and stimulated-emission (SE) cross-sections, σ_{SE}, for the $^5I_8 \leftrightarrow {}^5I_7$ Ho^{3+} transition. Light polarizations: π and σ.

In the visible, a weak and broad absorption band spanning from 400 to 650 nm is due to the residual color center absorption being typical for tetragonal double molybdates [46].

The polarized absorption cross-sections, σ_{abs}, corresponding to the $^3H_6 \rightarrow {}^3H_4$ transition of Tm^{3+} ions, were calculated from the measured absorption coefficient (α_{abs}), $\sigma_{abs} = \alpha_{abs}/N_{Tm}$. This spectral band well matches the emission of commercial high-power spatially multimode fiber-coupled AlGaAs laser diodes used as pump sources of Nd^{3+}-doped crystals. The maximum σ_{abs} is 3.41×10^{-20} cm^2 at 795.5 nm, corresponding to an absorption bandwidth (full width at half maximum, FWHM) of 6.6 nm for light polarization σ. For π-polarized light, the peak σ_{abs} is much lower, 1.31×10^{-20} cm^2 at 795.1 nm, but a broader absorption bandwidth of 15.7 nm is observed. In the previous studies [34, 37], the peak absorption cross-sections of Tm^{3+} ions in the NaGd$(MoO_4)_2$ crystal were found to lie in the range of $(3.85–5.2) \times 10^{-20}$ cm^2 for σ-polarized light and $(1.39–2.3) \times 10^{-20}$ cm^2 for π-polarization. The relatively broad absorption profile of Tm^{3+} ions around 0.8 μm is expected to mitigate the impact of temperature-induced drift of the pump diode emission wavelength.

The studied double molybdate crystal features higher absorption cross-sections for Tm^{3+} ions as compared to its double tungstate counterpart, $NaGd(WO_4)_2$, in which the maximum σ_{abs} for the $^3H_6 \rightarrow {}^3H_4$ transition is 2.9×10^{-20} cm^2 at 795 nm for light polarization σ (FWHM ~8 nm); at the same wavelength, σ_{abs} amounts to 1.18×10^{-20} cm^2 for π-polarized light [25].

5.2. Luminescence (spectra and lifetimes)

Fig. 6(a) depicts the polarized luminescence spectra of the Tm,Ho:$NaGd(MoO_4)_2$ crystal for light polarizations π and σ. For comparison, we also show the spectra measured for a singly Tm^{3+}-doped crystal. The broad emission band at 1.6–2.2 μm originates from two overlapping transitions: $^3F_4 \rightarrow {}^3H_6$ Tm^{3+} and $^5I_7 \rightarrow {}^5I_8$ Ho^{3+}. The studied crystal exhibits a strong anisotropy of emission properties, with higher intensity at 2.1 μm (Ho^{3+} emission) for π-polarized light. A strong spectral line broadening is observed, associated with the structure disorder of the host matrix. This results in smooth and broad emission profiles.

Fig. 6(b) illustrates the stimulated emission (SE) cross-sections, σ_{SE}, for the $^5I_7 \rightarrow {}^5I_8$ Ho^{3+} transition calculated using the Füchtbauer-Ladenburg equation [47]:

$$\sigma_{SE}^{i}(\lambda) = \frac{\lambda^5}{8\pi \langle n \rangle^2 \tau_{rad} c} \frac{W_i(\lambda)}{1 \Big/ 3 \sum_{j=2\sigma+\pi} \int \lambda' W_j(\lambda') d\lambda'}, \quad (1)$$

where λ is the luminescence wavelength, $<n>$ is the averaged (over polarization) refractive index at the central emission wavelength, τ_{rad} is the radiative lifetime of the $^5I_7$ Ho^{3+} state, c is the speed of light, and the indices i and $j = \sigma, \pi$ indicate the polarization state. In this calculation, we used the value of τ_{rad} of 6.0 ± 0.5 ms which provided the best agreement with the data obtained using the reciprocity method [48] based on the measured absorption spectrum. This estimate agrees well with the value of 6.61 ms determined using the Judd-Ofelt theory for an

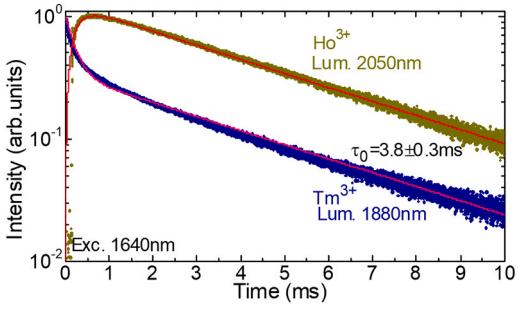

Fig. 8. Luminescence decay of Tm^{3+} and Ho^{3+} ions in $NaGd(MoO_4)_2$: a codoped crystal, decay from the $^3F_4$ Tm^{3+} and $^5I_7$ Ho^{3+} manifolds measured under resonant Tm^{3+} excitation: circles – experimental data, curves – their fits using Eq. (2).

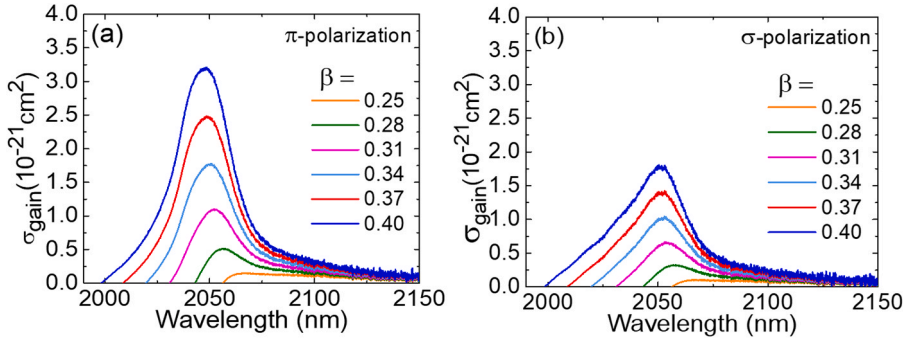

Fig. 7. Gain cross-sections, σ_{gain}, of the Ho^{3+} ion in the $NaGd(MoO_4)_2$ crystal: (a) light polarization π; (b) light polarization σ.

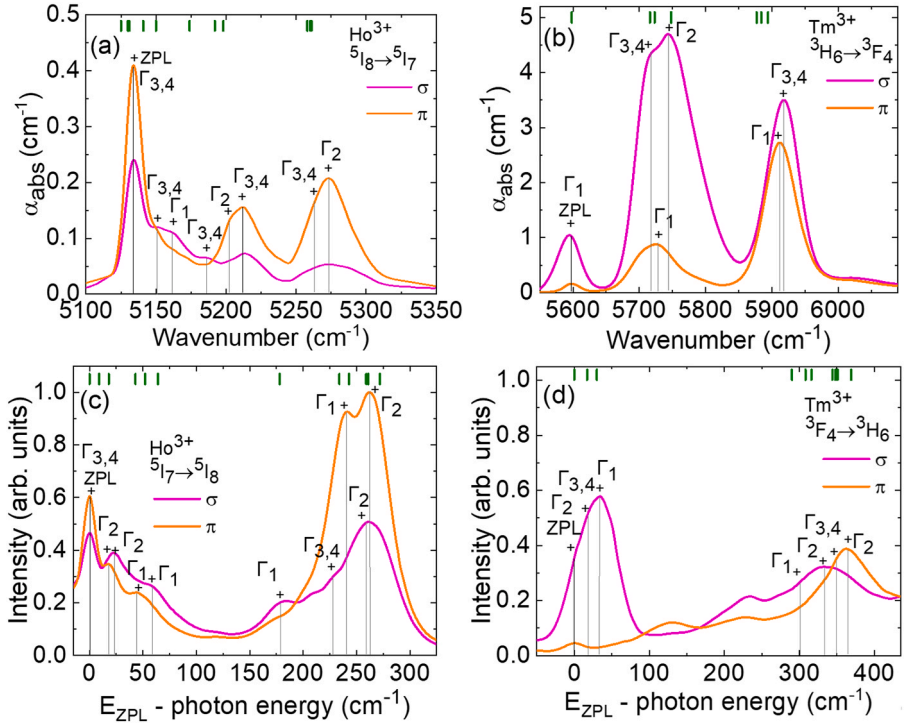

Fig. 9. Low-temperature (12 K) spectroscopy of Tm^{3+} and Ho^{3+} ions in $NaGd(MoO_4)_2$: (a,b) absorption: (a) the $^5I_8 \rightarrow {}^5I_7$ Ho^{3+} transition and (b) the $^3H_6 \rightarrow {}^3F_4$ Tm^{3+} transition; (c,d) luminescence: (c) the $^5I_7 \rightarrow {}^5I_8$ Ho^{3+} transition and (d) the $^3F_4 \rightarrow {}^3H_6$ Tm^{3+} transition. Light polarizations: π and σ. Vertical dashes – crystal-field calculations for isostructural crystals [27,51], vertical lines – assigned electronic transitions.

Table 4
Experimental crystal-field splitting (E_{exp}, in cm^{-1}) of selected Tm^{3+} and Ho^{3+} multiplets in $NaGd(MoO_4)_2$ in comparison with that for some scheelite-type molybdate crystals (E_{calc} – crystal-field calculation, Γ – irreducible representation).

Ho^{3+}	$NaGd(MoO_4)_2$	$NaBi(MoO_4)_2$ [27]			Tm^{3+}	$NaGd(MoO_4)_2$	$NaLa(MoO_4)_2$ [51]		
$^{2S+1}L_J$	E_{exp}	E_{exp}	E_{calc}	Γ	$^{2S+1}L_J$	E_{exp}	E_{exp}	E_{calc}	Γ
$^5I_8$	0	0	0	$\Gamma_{3,4}$	$^3H_6$	0	0	3	Γ_2
	18	9	9	Γ_2		19	-	17	$\Gamma_{3,4}$
	23	22	18	Γ_2		34	41	30	Γ_1
	44	45	43	Γ_1		-	280	290	Γ_2
	59	-	52	Γ_1		302	309	308	Γ_1
	-	72	64	$\Gamma_{3,4}$		-	-	316	$\Gamma_{3,4}$
	179	179	178	Γ_1		335	-	344	Γ_2
	228	233	234	$\Gamma_{3,4}$		349	-	348	$\Gamma_{3,4}$
	241	-	243	Γ_1		-	-	351	Γ_1
	259	-	259	Γ_2		364	-	369	Γ_2
	262	260	262	Γ_2		-	-	-	-
	-	-	272	Γ_1		-	-	-	-
$^5I_7$	-	-	5125	Γ_2	$^3F_4$	5595	5595	5598	Γ_1
	5133	5130	5130	$\Gamma_{3,4}$		5716	5707	5716	$\Gamma_{3,4}$
	-	-	5131	Γ_2		5728	5739	5723	Γ_1
	-	-	5141	Γ_1		5744	-	5748	Γ_2
	5150	-	5150	$\Gamma_{3,4}$		-	-	5877	Γ_2
	5162	5165	5174	Γ_1		5912	5881	5884	Γ_1
	5187	5193	5192	$\Gamma_{3,4}$		5918	5892	5894	$\Gamma_{3,4}$
	5202	5201	5198	Γ_2		-	-	-	-
	5212	5255	5258	$\Gamma_{3,4}$		-	-	-	-
	5263	5255	5260	Γ_2		-	-	-	-
	5273	-	5261	Γ_1		-	-	-	-

isostructural Ho:$NaLa(MoO_4)_2$ crystal [28].

The maximum SE cross-section σ_{SE} is 1.84×10^{-20} cm^2 at 2043 nm for π-polarized light (the corresponding emission bandwidth is 36 nm), and for σ-polarization, σ_{SE} is almost two times lower, 0.97×10^{-20} cm^2 at 2049 nm, while corresponding to a much broader emission profile (FWHM: 66 nm). The significant anisotropy of stimulated-emission properties suggests linearly polarized laser radiation in ***a***-cut crystals. As mentioned above, one of the key advantages of double molybdates consists of notably higher transition cross-sections for the dopant ions (as compared to their double tungstate counterparts). Sun *et al.* reported on polarized spectroscopy of a Ho:$NaY(WO_4)_2$ crystal yielding σ_{SE} of 1.43×10^{-20} cm^2 at 2047 nm for π-polarization supporting this statement [49] (note that the data for Ho:$NaGd(WO_4)_2$ are not available in the literature).

According to the quasi-three-level nature of the $^5I_7 \rightarrow {}^5I_8$ Ho^{3+} laser transition with reabsorption at the laser wavelength, we calculated the

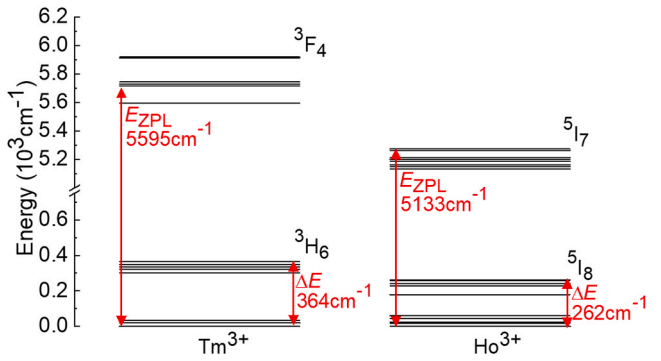

Fig. 10. Experimental crystal-field splitting of the two lowest multiplets of Tm^{3+} and Ho^{3+} ions in the $NaGd(MoO_4)_2$ crystal. E_{ZPL} – zero-phonon line energy.

gain cross-sections, $\sigma_{gain(Ho)} = \beta\sigma_{SE(Ho)} - (1 - \beta)\sigma_{abs(Ho)}$, for light polarizations π and σ, for the $NaGd(MoO_4)_2$ crystal, see Fig. 7. Here, β is the population inversion ratio, $\beta = N_2/N_{Ho}$ where N_2 is the density of ions excited to the upper laser level ($^5I_7$) and N_{Ho} is the total Ho^{3+} ion density. The gain profiles are nearly structureless which is a consequence of the inhomogeneous spectral line broadening inherent to this disordered compound. Higher gain is expected for π polarization. For $\beta > 0.25$, a local peak at 2.05 μm dominates in the spectra. When β reaches 0.40, the gain bandwidth (FWHM) is 31 nm, and the gain profile is peaking at 2048 nm. For σ-polarized light, at the same inversion level, the gain

Table 5
Output performance[a] of Tm,Ho lasers reported recently.

Crystal	P_{out}, mW	η, %	P_{th}, mW	λ_L, nm	Polariz.	Ref.
$KLu(WO_4)_2$	451	31	450	2081	$\boldsymbol{E} \parallel N_m$	[18]
$CaGdAlO_4$	1010	32	155	2081	π	[3]
CNGG	425	22.9	136	2084	Unpol.	[4]
$GdScO_3$	1160	50.5	184	2067, 2099	$\boldsymbol{E} \parallel \boldsymbol{c}$	[19]
$NaY(WO_4)_2$	265	43	~50	2050	π	[31]
$NaGd(MoO_4)_2$	548	32.4	98	2045–2055	π	This work

[a] P_{out} – output power, η - slope efficiency, P_{th} – laser threshold, λ_L – laser wavelength.

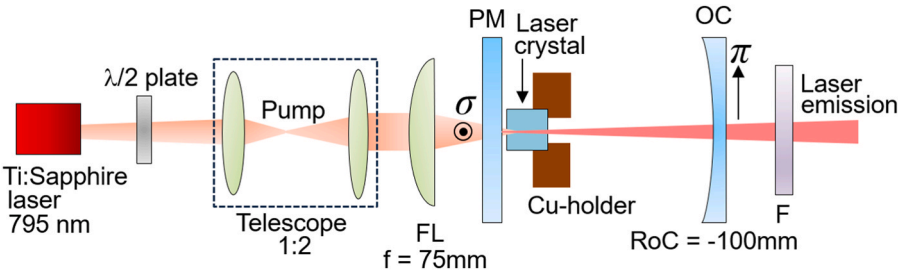

Fig. 11. Scheme of the Tm,Ho:$NaGd(MoO_4)_2$ laser: λ/2 - half-wave plate, FL - focusing lens, PM - pump mirror, OC - output coupler, F - long-pass filter.

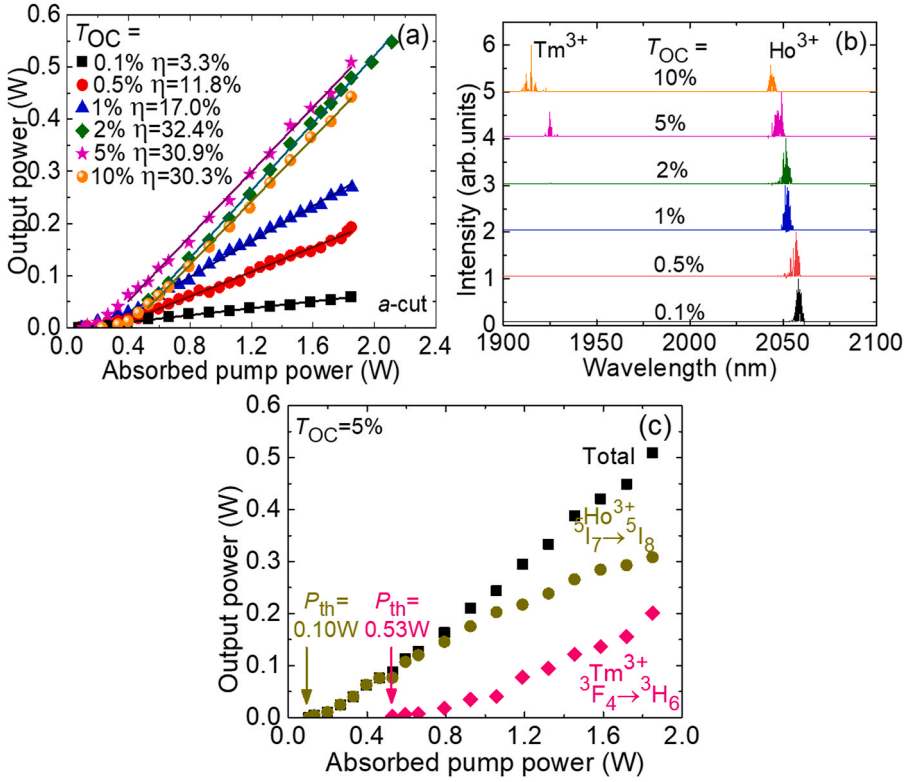

Fig. 12. Tm,Ho:$NaGd(MoO_4)_2$ laser: (a) input-output dependences for different output coupling rates, η – slope efficiency; (b) laser emission spectra measured well above the laser threshold, π-polarization; (c) Tm^{3+} and Ho^{3+} colasing for T_{OC} = 5 %. **a**-cut crystal.

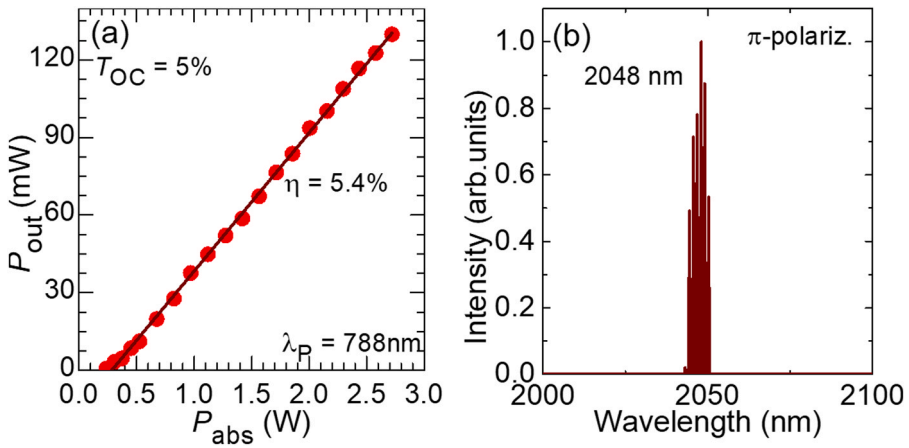

Fig. 13. Diode-pumped Tm,Ho:NaGd$(MoO_4)_2$ laser: (a) input-output dependences, η – slope efficiency; (b) a typical laser emission spectrum, π-polarization. T_{OC} = 5 %.

maximum is found at 2051 nm and the gain profile is broader (FWHM: 35 nm), offering better possibilities for wavelength tuning and ultrashort pulse generation.

The luminescence dynamics from the excited states of Tm^{3+} and Ho^{3+} ions in NaGd$(MoO_4)_2$, which are responsible for emission around 2 μm, was studied under resonant excitation of Tm^{3+} (at 1640 nm, to the $^3F_4$ state). The luminescence was detected at two wavelengths corresponding to almost pure Tm^{3+} (1880 nm) and Ho^{3+} (2050 nm) emission. The luminescence decay curves from the $^3F_4$ Tm^{3+} and $^5I_7$ Ho^{3+} manifolds are plotted in a semi-log scale in Fig. 8. Shortly after the excitation pulse, a rapid rise of the Ho^{3+} emission intensity is observed and at the same time, a fast drop in the intensity of Tm^{3+} luminescence is evident. These phenomena are indicative of a direct energy transfer from Tm^{3+} (donor, D) to Ho^{3+} (acceptor, A). At longer time scales, the decay rates from the $^3F_4$ Tm^{3+} and $^5I_7$ Ho^{3+} manifolds become identical as a thermal equilibrium is reached between them, balancing the direct and back energy transfer.

The parameters of the bidirectional $^3F_4(Tm^{3+}) \leftrightarrow {}^5I_7(Ho^{3+})$ energy-transfer were determined using the dynamical model developed by Walsh *et al.* [50]. The luminescence decay curves were fitted using the following equations:

$$\frac{n_2(t)}{n_2(0)} = \frac{\beta}{\alpha+\beta}\exp\left(-\frac{t}{\tau}\right) + \frac{\alpha}{\alpha+\beta}\exp\left(-\left(\alpha+\beta\right)t\right), \quad (2a)$$

$$\frac{n_7(t)}{n_7(0)} = \frac{\beta}{\alpha+\beta}\exp\left(-\frac{t}{\tau}\right) - \frac{\alpha}{\alpha+\beta}\exp\left(-\left(\alpha+\beta\right)t\right), \quad (2b)$$

where t is time after a short-pulse excitation, τ is the thermal equilibrium decay time, n_2 and n_7 are the populations of the $^3F_4$ Tm^{3+} and $^5I_7$ Ho^{3+} manifolds, respectively (here, we assume that the luminescence intensity is proportional to electronic populations), $\alpha = P_{28}N_{Ho}$ and $\beta = P_{71}N_{Tm}$ are the transfer rates, P_{28} is a parameter of a direct nonradiative energy transfer, $Tm^{3+} \rightarrow Ho^{3+}$, and P_{71} is a parameter of the back nonradiative energy transfer, $Ho^{3+} \rightarrow Tm^{3+}$. The best-fit curves are shown in Fig. 8. The best-fit parameters are $\tau = 3.80 \pm 0.3$ ms, $P_{28} = 1.09 \pm 0.05 \times 10^{-22}$ $cm^3\mu s^{-1}$ and $P_{71} = 0.42 \pm 0.05 \times 10^{-23}$ $cm^3\mu s^{-1}$. The ratio of the energy-transfer parameters, $\Theta = P_{71}/P_{28}$, also known as the equilibrium constant, is relatively small, 0.038. This value confirms the predominantly direct $Tm^{3+} \rightarrow Ho^{3+}$ energy transfer.

The luminescence decay curve for a singly doped 5 at% Tm:NaGd$(MoO_4)_2$ crystal was also studied for comparison yielding a luminescence lifetime of the $^3F_4$ and $^3H_4$ Tm^{3+} states τ_{lum} of 1.41 ms and 30 μs, respectively. The measured $^3F_4$ lifetime is longer than that determined in the previous studies (1.2 ms) [34,37], as well as the previously reported radiative lifetime, calculated using the Judd-Ofelt theory (0.9 ms) [37], which is probably due to the residual effect of reabsorption (radiation trapping). The relatively short luminescence lifetime of the $^3H_4$ state indicates an efficient cross-relaxation among adjacent ions contributing to enhanced pump quantum efficiency.

5.3. Low temperature spectroscopy

The polarized absorption and emission spectra corresponding to the $^3H_6 \leftrightarrow {}^3F_4$ Tm^{3+} and $^5I_8 \leftrightarrow {}^5I_7$ Ho^{3+} transitions in the studied crystal were acquired at low temperature (LT, 12 K). The results are shown in Fig. 9. The LT absorption spectra gave access to the crystal-field splitting of excited-states, and they were expressed in photon energy (in cm^{-1}). The LT emission spectra were analyzed to resolve the Stark sub-level energies of the ground-states, plotted as a function of (E_{ZPL} - photon energy), where E_{ZPL} is the zero-phonon line (ZPL) energy. Here, ZPL indicates the transitions between the lowest-lying Stark sub-levels of both multiplets.

The trivalent dopant ions in the NaGd$(MoO_4)_2$ crystal reside in the ($Na^+ + Gd^{3+}$) site of the scheelite structure with S_4 symmetry (Wyckoff: 4*b*). For the tetragonal crystal field, any multiplet $^{2S+1}L_J$ with an integer total angular momentum J of 4, 6, 7 and 8 will be split into 7, 10, 11 and 13 Stark components, respectively. In this study, we determined the crystal-field splitting of the two lowest multiplets of Tm^{3+} ($^3H_6$ and $^3F_4$) and Ho^{3+} ($^5I_8$ and $^5I_7$) in NaGd$(MoO_4)_2$, relevant for describing their laser emission properties around 2 μm. For assignment of electronic transitions, we followed the crystal-field data reported previously for Tm^{3+} in NaLa$(MoO_4)_2$ [51] and Ho^{3+} in NaBi$(MoO_4)_2$ [27] (both crystals adopt the same tetragonal structure as NaGd$(MoO_4)_2$ studied in the present work). The electronic transitions for these reference crystals are marked with vertical dashes in Fig. 9.

Table 4 lists the experimental energies of Stark sub-levels of ($^3H_6$ and $^3F_4$) Tm^{3+} and ($^5I_8$ and $^5I_7$) Ho^{3+} multiplets in NaGd$(MoO_4)_2$. Fig. 10 illustrates the corresponding energy-level schemes. The ZPL transition for both ions is indicated. For Tm^{3+}, it occurs at 1787.3 nm, corresponding to an energy E_{ZPL} of 5595 cm^{-1}, whereas for Ho^{3+}, it is expected at 1948 nm (E_{ZPL} = 5133 cm^{-1}). The total Stark splitting of the ground-state amounts to $\Delta E(^3H_6)$ = 364 cm^{-1} for Tm^{3+} and $\Delta E(^5I_8)$ = 262 cm^{-1} for Ho^{3+}.

6. Laser operation

The scheme of the laser cavity is depicted in Fig. 11. The rectangular laser element was cut from the annealed Tm,Ho:NaGd$(MoO_4)_2$ crystal for light propagation along the ***a***-axis (***a***-cut) and it was 3.0 mm-thick with an aperture of 3.0(***c***)× 3.0 mm^2. Both its input and output surfaces were polished to laser grade quality with good parallelism and antireflection (AR) coated for both the pump and laser wavelengths. The

crystal was mounted on a passively cooled Cu-holder using a silver paint for better heat management. The hemispherical cavity was formed by a plane pump mirror (PM) coated for high transmission (HT) at 0.8 μm and high reflection (HR, $R > 99.9$ %) at 1.85 – 2.3 μm, and a set of concave output couplers (OCs) having a radius of curvature (RoC) of −100 mm and a transmission at the laser wavelength T_{OC} ranging from 0.1 % to 10 %. The crystal was placed near the PM leaving only a small air gap (<1 mm) and the geometrical cavity length was about 99 mm. The pump source was a Ti:Sapphire laser (3900S, Spectra Physics) delivering up to 3.2 W at 795 nm with a nearly diffraction limited beam ($M^2 \approx 1$). The pump polarization was adjusted using an AR-coated half-wave plate to correspond to σ in the crystal. The pump beam was focused into the crystal through the PM using an AR-coated achromatic lens (focal length: f = 75 mm). The single-pass pump absorption efficiency under lasing conditions was weakly dependent on the output coupling, amounting to 96 %. The spectra of laser emission were measured by the same optical spectrum analyzer and a multimode ZrF_4 fiber.

The continuous-wave Tm,Ho:$NaGd(MoO_4)_2$ laser generated a maximum output power of 548 mW at 2045 – 2055 nm corresponding to a slope efficiency η of 32.4 % (relative to the absorbed pump power), and a laser threshold of 98 mW, see Fig. 12(a). This performance was achieved through an intermediate output coupling ($T_{OC} = 2$ %). The laser output corresponded to pure Ho^{3+} emission (the $^5I_7 \rightarrow {}^5I_8$ transition). For higher output coupling, the laser slope efficiency slightly decreased (to 30.9 % for 5 % OC and then to 30.3 % for 10 % OC). On increasing the output coupling from 0.1 % to 10 %, the laser threshold progressively increased from 74 mW to 227 mW. Well above the laser threshold, the input-output dependencies were linear. Up to the absorbed pump power of about 2 W, neither signs of undesired thermal effects nor crystal fracture were observed. Further power scaling was limited by the power provided by the Ti:Sapphire laser.

Fig. 12(b) illustrates typical laser emission spectra measured for all the studied OCs well above the laser threshold. For low output coupling ($T_{OC} \leq 2$ %), the Tm,Ho-laser operated solely on the $^5I_7 \rightarrow {}^5I_8$ Ho^{3+} transition without Tm^{3+} colasing. Conversely, higher output coupling ($T_{OC} \geq 5$ %) facilitated colasing at about 1.92 μm ($^3F_4 \rightarrow {}^3H_6$, Tm^{3+}) and 2.04 μm ($^5I_7 \rightarrow {}^5I_8$, Ho^{3+}). The laser emission in all cases was linearly polarized (π), and the polarization state was determined by the anisotropy of the gain. Regarding Ho^{3+} emission, a notable blue-shift in the emission spectra was observed with increasing the output coupling, attributed to the quasi-three-level nature of the $^5I_7 \rightarrow {}^5I_8$ Ho^{3+} laser scheme involving reabsorption from the terminal laser level.

Fig. 12(c) shows the power redistribution between Ho^{3+} and Tm^{3+} emissions with increasing the absorbed pump power under high output coupling ($T_{OC} = 5$ %). First, the Ho-laser starts to operate with a threshold of 100 mW. Above 530 mW of absorbed pump power, the Tm laser emission appears in addition and the slope efficiency of the Ho-laser decreases. The power fractions of Ho^{3+} and Tm^{3+} emissions almost equalize at high pump powers.

The laser performance achieved for the Tm,Ho:$NaGd(MoO_4)_2$ crystal in the present work is superior to the previous results for Tm,Ho-lasers based on scheelite-type tetragonal tungstate and molybdate crystals. Han *et al.* reported on a continuous-wave Tm,Ho:$NaY(WO_4)_2$ laser delivering 265 mW at 2050 nm with a slope efficiency of 43 % and π-polarized emission [31]. The same authors explored a Tm,Ho:$NaLu(WO_4)_2$ crystal generating only 50 mW at 2060 nm for σ-polarization [31]. Dunaeva *et al.* developed a diode-pumped Tm,Ho:$SrMoO_4$ laser generating 1.63 mW at 2060 nm with η of 3 % and a laser threshold of 40 mW [52].

The output characteristics of Tm,Ho lasers with Ti:Sapphire laser pumping reported recently are compared in Table 5. The studied laser features a reasonably high slope efficiency (~30 %) comparable to those observed previously for state-of-the-art laser materials such as Tm^{3+}, Ho^{3+}-codoped $KLu(WO_4)_2$ and $CaGdAlO_4$, and benefits from a very low laser threshold (~100 mW). The latter is assigned to the relatively long thermal equilibrium luminescence lifetime, as well as low intracavity losses in part due to the AR coatings applied on the crystal.

We further applied a fiber-coupled (fiber core diameter: 105 μm, N. A. = 0.22) AlGaAs laser diode (*DILAS*) emitting at 788 nm for pumping the Tm,Ho:$NaGd(MoO_4)_2$ crystal. The diode output was reimagined into the crystal using a pair of AR-coated achromatic lenses ($f = 40$ mm and 50 mm, respectively). The above-described laser cavity was used. The absorption efficiency of unpolarized pump was about 48 %. The output characteristics of the diode-pumped Tm,Ho-laser are presented in Fig. 13. For $T_{OC} = 5$ %, we achieved a maximum output power of 130 mW at 2048 nm with a slope efficiency of 5.4 % and a laser threshold of 233 mW. These results highlight the potential of the developed material for diode-pumped laser systems.

7. Conclusion

To conclude, Tm^{3+},Ho^{3+}-codoped sodium gadolinium double molybdate ($NaGd(MoO_4)_2$) crystals hold promise for ultrashort pulse and broadly tunable laser sources emitting in the eye-safe spectral range, above 2 μm. The main feature of this compound belonging to the crystal family of tetragonal scheelite-type double tungstates / molybdates is a strong inhomogeneous spectral line broadening in the absorption and emission spectra stemming from the structure disorder. It mitigates the requirements for wavelength stabilization of pump sources (e.g., laser diodes), as well as enables smooth and broad gain profiles around 2 μm (gain bandwidth: 66 nm for σ-polarized light) supporting generation of sub-100 fs pulses from mode-locked lasers, as well as broadband tuning of laser emission. This compound also benefits from a strong polarization anisotropy of emission properties enabling linearly polarized laser radiation. The $Tm^{3+} \rightarrow Ho^{3+}$ energy transfer in this double molybdate crystal is very efficient, alongside a relatively long thermal equilibrium decay time leading to low laser thresholds. As compared to tetragonal double tungstates, the studied crystal features higher transition cross-sections for the dopant ions. The aforementioned appealing spectroscopic properties allowed us to demonstrate efficient and low-threshold continuous-wave laser action in Tm:Ho:$NaGd(MoO_4)_2$.

CRediT authorship contribution statement

Camy Patrice: Supervision, Funding acquisition. **Slimi Sami:** Investigation. **Braud Alain:** Methodology. **Aguiló Magdalena:** Supervision, Funding acquisition. **Pan Zhongben:** Writing – original draft, Investigation. **Solé Rosa Maria:** Methodology. **Zin Elabedine Ghassen:** Writing – original draft, Investigation. **Chen Weidong:** Conceptualization. **Chu Hongwei:** Investigation. **Díaz Francesc:** Supervision, Funding acquisition. **Loiko Pavel:** Writing – original draft, Methodology, Conceptualization. **Petrov Valentin:** Writing – review & editing, Methodology. **Eremeev Kirill:** Investigation. **Griebner Uwe:** Writing – review & editing. **Li Dechun:** Investigation. **Pavlov Sergei:** Investigation. **Mateos Xavier:** Writing – review & editing, Supervision, Funding acquisition. **Subbotin Kirill:** Resources, Investigation.

Declaration of Competing Interest

The authors declare that they have no known competing financial interests or personal relationships that could have appeared to influence the work reported in this paper.

Acknowledgements

Grant PECT “Cuidem el que ens uneix”, operació 4 sensòrica, Act 4 Fotònica” PR15–020174 co-financed by the European Regional Development Fund “ERDF A way of making Europe” through the ERDF Catalonia Operational Programme 2014–2020. Project PID2022–141499OB-100, funded by MICIU/AEI/10.13039/501100011033/ and by FEDER/UE. Russian Science Foundation (grant 23–22–00416). National Natural Science Foundation of China (project

No. 52072351).

Data availability

Data will be made available on request.

References

[1] J. Ma, Z. Qin, G. Xie, L. Qian, D. Tang, Review of mid-infrared mode-locked laser sources in the 2.0 μm-3.5 μm spectral region, Appl. Phys. Rev. 6 (2019) 21317, https://doi.org/10.1063/1.5037274/570142.

[2] C.W. Rudy, M.J.F. Digonnet, R.L. Byer, Advances in 2-μm Tm-doped mode-locked fiber lasers, Opt. Fiber Technol. 20 (2014) 642–649, https://doi.org/10.1016/J.YOFTE.2014.06.005.

[3] Y. Wang, P. Loiko, Y. Zhao, Z. Pan, W. Chen, M. Mero, X. Xu, J. Xu, X. Mateos, X. Mateos, A. Major, M. Guina, V. Petrov, U. Griebner, Polarized spectroscopy and SESAM mode-locking of Tm,Ho:CALGO, Opt. Express 30 (2022) 7883–7893, https://doi.org/10.1364/OE.449626.

[4] Z. Pan, P. Loiko, Y. Wang, Y. Zhao, H. Yuan, K. Tang, X. Dai, H. Cai, J.M. Serres, S. Slimi, E. Ben Salem, E. Dunina, A. Kornienko, L. Fomicheva, J.L. Doualan, P. Camy, W. Chen, U. Griebner, V. Petrov, M. Aguiló, F. Díaz, R.M. Solé, X. Mateos, Disordered Tm^{3+},Ho^{3+}-codoped CNGG garnet crystal: towards efficient laser materials for ultrashort pulse generation at ~2 μm, J. Alloy. Compd. 853 (2021) 157100, https://doi.org/10.1016/J.JALLCOM.2020.157100.

[5] P.O. Petit, J. Petit, P. Goldner, B. Viana, Inhomogeneous broadening of optical transitions in Yb:$CaYAlO_4$, Opt. Mater. 30 (2008) 1093–1097, https://doi.org/10.1016/J.OPTMAT.2007.05.017.

[6] J.M. Cano-Torres, M. Rico, X. Han, M.D. Serrano, C. Cascales, C. Zaldo, V. Petrov, U. Griebner, X. Mateos, P. Koopmann, C. Kränkel, Comparative study of crystallographic, spectroscopic, and laser properties of Tm^{3+} in $NaT(WO_4)_2$ (T=La, Gd, Y, and Lu) disordered single crystals, Phys. Rev. B 84 (2011) 174207, https://doi.org/10.1103/PHYSREVB.84.174207.

[7] A.A. Lagatsky, X. Han, M.D. Serrano, C. Cascales, C. Zaldo, S. Calvez, M.D. Dawson, J.A. Gupta, C.T.A. Brown, W. Sibbett, Femtosecond (191 fs) $NaY(WO_4)_2$ Tm,Ho-codoped laser at 2060 nm, Opt. Lett. 35 (2010) 3027–3029, https://doi.org/10.1364/OL.35.003027.

[8] A. Schmidt, S. Rivier, V. Petrov, U. Griebner, X. Han, J.M. Cano-Torres, A. García-Cortés, M.D. Serrano, C. Cascales, C. Zaldo, Continuous-wave tunable and femtosecond mode-locked laser operation of Yb:$NaY(MoO_4)_2$, J. Opt. Soc. Am. B 25 (2008) 1341–1349, https://doi.org/10.1364/JOSAB.25.001341.

[9] C. Cascales, M.D. Serrano, F. Esteban-Betegón, C. Zaldo, R. Peters, K. Petermann, G. Huber, L. Ackermann, D. Rytz, C. Dupré, M. Rico, J. Liu, U. Griebner, V. Petrov, Structural, spectroscopic, and tunable laser properties of Yb^{3+}-doped $NaGd(WO_4)_2$, Phys. Rev. B. 74 (2006) 174114, https://doi.org/10.1103/PhysRevB.74.174114.

[10] G.M. Kuz'micheva, V.B. Rybakov, V.L. Panyutin, E.V. Zharikov, K.A. Subbotin, Symmetry of $(Na_{0.5}R_{0.5})MO_4$ crystals (R = Gd, La; M = W, Mo), Russ. J. Inorg. Chem. 55 (2010) 1448–1453, https://doi.org/10.1134/S0036023610090196.

[11] B.G. Mullens, M.K. Nicholas, F.P. Marlton, H.E.A. Brand, Q. Gu, H.E. Maynard-Casely, B.J. Kennedy, Long-range A-site cation disorder in $NaA(MO_4)_2$ (M = Mo, W) double scheelite oxides, J. Solid State Chem. 321 (2023) 123871, https://doi.org/10.1016/j.jssc.2023.123871.

[12] X. Han, A. García-Cortés, M.D. Serrano, C. Zaldo, C. Cascales, Structural and thermal properties of tetragonal double tungstate crystals intended for ytterbium laser composites, Chem. Mater. 19 (2007) 3002–3010, https://doi.org/10.1021/cm070237v.

[13] X. Han, D.E. Lahera, M.D. Serrano, C. Cascales, C. Zaldo, Ultraviolet to infrared refractive indices of tetragonal double tungstate and double molybdate laser crystals, Appl. Phys. B 108 (2012) 509–514, https://doi.org/10.1007/S00340-012-4936-6.

[14] A.A. Kaminskii, H.J. Eichler, K. Ueda, N.V. Klassen, B.S. Redkin, L.E. Li, J. Findeisen, D. Jaque, J. García-Sole, J. Fernández, R. Balda, Properties of Nd^{3+}-doped and undoped tetragonal $PbWO_4$, $NaY(WO_4)_2$, $CaWO_4$, and undoped monoclinic $ZnWO_4$ and $CdWO_4$ as laser-active and stimulated Raman scattering-active crystals, Appl. Opt. 38 (1999) 4533–4547, https://doi.org/10.1364/AO.38.004533.

[15] J. Fan, H. Zhang, J. Wang, Z. Ling, H. Xia, X. Chen, Y. Yu, Q. Lu, M. Jiang, Growth, structure and thermal properties of Yb^{3+}-doped $NaGd(WO_4)_2$ crystal, J. Phys. D Appl. Phys. 39 (2006) 1034, https://doi.org/10.1088/0022-3727/39/6/007.

[16] P.A. Loiko, X. Han, K.V. Yumashev, N.V. Kuleshov, M.D. Serrano, C. Cascales, C. Zaldo, Thermo-optical properties of uniaxial $NaT(XO_4)_2$ laser host crystals (where T = Y, La, Gd or Bi, and X = W or Mo), Appl. Phys. B 111 (2013) 279–287, https://doi.org/10.1007/S00340-012-5331-Z.

[17] T.Y. Fan, G. Huber, R.L. Byer, P. Mitzscherlich, Spectroscopy and diode laser-pumped operation of Tm, Ho: YAG, IEEE J. Quantum Electron. 24 (1988) 924–933, https://doi.org/10.1109/3.213.

[18] P. Loiko, J.M. Serres, X. Mateos, K. Yumashev, N. Kuleshov, V. Petrov, U. Griebner, M. Aguiló, F. Díaz, Microchip laser operation of Tm,Ho:$KLu(WO_4)_2$ crystal, Opt. Express 22 (2014) 27976–27984, https://doi.org/10.1364/OE.22.027976.

[19] K. Eremeev, P. Loiko, C. Zhao, Z.-L. Lin, X. Mateos, G.Z. Elabedine, P. Camy, A. Braud, U. Griebner, V. Petrov, G. Zhang, S. Li, Y. Hang, W. Chen, W. Chen, Growth, spectroscopy and laser operation of Tm,Ho:$GdScO_3$ perovskite crystal, Opt. Express 32 (2024) 13527–13542, https://doi.org/10.1364/OE.518709.

[20] Y. Zhao, Y. Wang, X. Zhang, X. Mateos, Z. Pan, P. Loiko, W. Zhou, X. Xu, J. Xu, D. Shen, S. Suomalainen, A. Härkönen, M. Guina, U. Griebner, V. Petrov, 87 fs mode-locked Tm,Ho:$CaYAlO_4$ laser at ~2043 nm, Opt. Lett. 43 (2018) 915–918, https://doi.org/10.1364/OL.43.000915.

[21] Y. Zhao, Y. Wang, W. Chen, Z. Pan, L. Wang, X. Dai, H. Yuan, Y. Zhang, H. Cai, J. E. Bae, S.Y. Choi, F. Rotermund, P. Loiko, J.M. Serres, X. Mateos, W. Zhou, D. Shen, U. Griebner, V. Petrov, 67-fs pulse generation from a mode-locked Tm,Ho:CLNGG laser at 2083 nm, Opt. Express 27 (2019) 1922–1928, https://doi.org/10.1364/OE.27.001922.

[22] A. Gluth, Y. Wang, V. Petrov, J. Paajaste, S. Suomalainen, A. Härkönen, M. Guina, G. Steinmeyer, X. Mateos, S. Veronesi, M. Tonelli, J. Li, Y. Pan, J. Guo, U. Griebner, GaSb-based SESAM mode-locked Tm:YAG ceramic laser at 2 μm, Opt. Express 23 (2015) 1361–1369, https://doi.org/10.1364/OE.23.001361.

[23] W. Guo, Y. Chen, Y. Lin, X. Gong, Z. Luo, Y. Huang, Spectroscopic analysis and laser performance of Tm^{3+}:$NaGd(MoO_4)_2$ crystal, J. Phys. D Appl. Phys. 41 (2008) 115409, https://doi.org/10.1088/0022-3727/41/11/115409.

[24] X. Han, M. Rico, M.D. Serrano, C. Cascales, C. Zaldo, Efficient infrared (≈1.9–2.0 μm) laser operation in color-defect-free Tm:$NaGd(MoO_4)_2$ crystal, Laser Phys. Lett. 10 (2013) 045808, https://doi.org/10.1088/1612-2011/10/4/045808.

[25] J.M. Cano-Torres, M.D. Serrano, C. Zaldo, M. Rico, X. Mateos, J. Liu, U. Griebner, V. Petrov, F.J. Valle, M. Galán, G. Viera, Broadly tunable laser operation near 2μm in a locally disordered crystal of Tm^{3+}-doped $NaGd(WO_4)_2$, J. Opt. Soc. Am. B 23 (2006) 2494–2502, https://doi.org/10.1364/JOSAB.23.002494.

[26] L. Zhang, S. Sun, Z. Lin, H. Lin, G. Zhang, X. Mateos, J.M. Serres, M. Aguiló, F. Díaz, P. Loiko, Y. Wang, U. Griebner, V. Petrov, E. Vilejshikova, W. Chen, Crystal growth, spectroscopy and first laser operation of a novel disordered tetragonal Tm:$Na_2La_4(WO_4)_7$ tungstate crystal, J. Lumin. 203 (2018) 676–682, https://doi.org/10.1016/J.JLUMIN.2018.07.016.

[27] A. Méndez-Blas, M. Rico, V. Volkov, C. Zaldo, C. Cascales, Crystal field analysis and emission cross sections of Ho^{3+} in the locally disordered single-crystal laser hosts $M^{+}Bi(XO_4)_2$ (M^{+}=Li,Na; X=W,Mo), Phys. Rev. B 75 (2007) 174208, https://doi.org/10.1103/PHYSREVB.75.174208.

[28] C.H. Cheng, X.H. Gong, Y.F. Lin, Z.D. Luo, Y.J. Chen, J.H. Huang, Y.D. Huang, Polarized spectroscopic properties of Ho^{3+} ions in $NaLa(MoO_4)_2$ crystal, Opt. Mater. 33 (2011) 763–767, https://doi.org/10.1016/J.OPTMAT.2010.12.010.

[29] C. Wang, H. Yin, A. Li, Y. Wu, S. Zhu, Z. Chen, G. Zhang, K. Su, Growth, thermal and spectral properties of Tm^{3+}, Ho^{3+} co-doped $NaGd(MoO_4)_2$ Crystal, J. Alloy. Compd. 615 (2014) 482–487, https://doi.org/10.1016/J.JALLCOM.2014.06.084.

[30] J. Tang, Y. Chen, Y. Lin, X. Gong, J. Huang, Z. Luo, Y. Huang, Tm^{3+}/Ho^{3+} co-doped $LiGd(MoO_4)_2$ crystal as laser gain medium around 2.0 μm, Opt. Mater. Express 2 (2012) 1064–1075, https://doi.org/10.1364/OME.2.001064.

[31] X. Han, F. Fusari, M.D. Serrano, A.A. Lagatsky, J.M. Cano-Torres, C.T.A. Brown, C. Zaldo, W. Sibbett, Continuous-wave laser operation of Tm and Ho co-doped $NaY(WO_4)_2$ and $NaLu(WO_4)_2$ crystals, Opt. Express 18 (2010) 5413–5419, https://doi.org/10.1364/OE.18.005413.

[32] X. Li, Z. Lin, L. Zhang, G. Wang, Growth, thermal and spectral properties of Nd^{3+}-doped $NaGd(MoO_4)_2$ crystal, J. Cryst. Growth 290 (2006) 670–673, https://doi.org/10.1016/J.JCRYSGRO.2006.02.005.

[33] Y.K. Voron'ko, K.A. Subbotin, V.E. Shukshin, D.A. Lis, S.N. Ushakov, A.V. Popov, E. V. Zharikov, Growth and spectroscopic investigations of Yb^{3+}-doped $NaGd(MoO_4)_2$ and $NaLa(MoO_4)_2$—new promising laser crystals, Opt. Mater. 29 (2006) 246–252, https://doi.org/10.1016/J.OPTMAT.2005.09.004.

[34] Yu.K. Voron'ko, E.V. Zharikov, D.A. Lis, A.V. Popov, V.A. Smirnov, K.A. Subbotin, Spectroscopy of $NaLa(MoO_4)_2$:Tm^{3+} and $NaGd(MoO_4)_2$:Tm^{3+} crystals as advanced laser materials, Phys. Sol. State 50 (2008) 1605–1610, https://doi.org/10.1134/S1063783408090023.

[35] Z. Wang, X. Li, G. Wang, M. Song, Q. Wei, G. Wang, X. Long, Growth and optical properties of Ho^{3+}:$NaGd(MoO_4)_2$ crystal, Opt. Mater. 30 (2008) 1873–1877, https://doi.org/10.1016/J.OPTMAT.2007.12.012.

[36] A. Li, J. Li, Z. Chen, Y. Wu, L. Wu, G. Liu, G, C. Wang, G. Zhang, Growth and spectral properties of Yb^{3+}/Ho^{3+} co-doped $NaGd(MoO_4)_2$ crystal, Mater. Express 5 (2015) 527–533, https://doi.org/10.1166/mex.2015.1269.

[37] F.A. Bolschikov, E.V. Zharikov, D.A. Lis, A.V. Popov, P.A. Ryabochkina, V.G. Senin, K.A. Subbotin, Growth, optical parameters, and spectroscopic properties of crystals of disordered scheelite-like molybdates $NaLa_xGd_{1-x}(MoO_4)_2$ (x = 0-1) activated by Tm^{3+} ions, Opt. Spectrosc. 108 (2010) 743–752, https://doi.org/10.1134/S0030400X10050127.

[38] F.A. Bolschikov, E.V. Zharikov, D.A. Lis, N.G. Zakharov, P.A. Ryabochkina, K. A. Subbotin, O.L. Antipov, Tunable quasi-cw two-micron lasing in diode-pumped crystals of mixed Tm^{3+}-doped sodium - lanthanum - gadolinium molybdates and tungstates, Quantum Electron 40 (2010) 847–850, https://doi.org/10.1070/QE2010v040n10ABEH014403.

[39] F. Cheng, Z. Xia, M.S. Molokeev, X. Jing, Effects of composition modulation on the luminescence properties of Eu^{3+} doped $Li_{1-x}Ag_xLu(MoO_4)_2$ solid-solution phosphors, Dalton Trans. 44 (2015) 18078–18089, https://doi.org/10.1039/C5DT02760H.

[40] O.D. Chimitova, V.V. Atuchin, B.G. Bazarov, M.S. Molokeev, Z.G. BazarovaThe formation and structural parameters of new double molybdates RbLn(MoO4)2 (Ln= Pr, Nd, Sm, Eu), Proc. SPIE, 87711A, 10.1117/12.20178162013.

[41] D.K. Amarasinghe, S.S. Perera, F.A. Rabuffetti, Rotational disorder in scheelite-type $NaRE(MO_4)_2$ (RE = Rare-Earth, Y; M = Mo, W), Cryst. Growth Des. 20 (2020) 3442–3448, https://doi.org/10.1021/ACS.CGD.0C00225.

[42] S. Perets, R.Z. Shneck, R. Gajic, A. Golubovic, Z. Burshtein, Vibrational spectra of sodium gadolinium tungstate $NaGd(WO_4)_2$ single crystals: observation of spatial dispersion, Vib. Spectrosc. 49 (2009) 110–117, https://doi.org/10.1016/j.vibspec.2008.05.006.

[43] W.T. Carnall, P.R. Fields, K. Rajnak, Electronic energy levels in the trivalent lanthanide Aquo Ions. I. Pr^{3+}, Nd^{3+}, Pm^{3+}, Sm^{3+}, Dy^{3+}, Ho^{3+}, Er^{3+}, and Tm^{3+}, J. Chem. Phys. 49 (1968) 4424–4442, https://doi.org/10.1063/1.1669893.

[44] Q. Wu, H. Li, W. Xia, X. Fu, Z. Fu, S. Zhou, S. Zhang, J.H. Jeong, Investigation of the structure and photoluminescence properties of Ln^{3+}(Eu^{3+}, Dy^{3+}, Sm^{3+}) ion-doped $NaY(MoO_4)_2$, J. Electrochem. Soc. 158 (2011) J387, https://doi.org/10.1149/2.012112jes.

[45] A. Khomyakov, E. Sukhanova, E. Mozhevitina, M. Zykova, A. Barkanov, R. Avetisov, A. Yurkin, K. Subbotin, O. Lis, I. Avetissov, Effect of high purity molybdenum oxide (VI) on crystal growth and OLED technology, CrystEngComm 23 (2021) 8276–8290, https://doi.org/10.1039/d1ce01322j.

[46] G.M. Kuz'micheva, V.B. Rybakov, K.A. Subbotin, E.V. Zharikov, D.A. Lis, O. Zaharko, D.A. Nikolaev, V.G. Senin, Colors of mixed-substituted double molybdate single crystals having scheelite structure, Russ. J. Inorg. Chem. 57 (2012) 1128–1133, https://doi.org/10.1134/S0036023612080098.

[47] B.F. Aull, H.P. Jenssen, Vibronic interactions in Nd: YAG resulting in nonreciprocity of absorption and stimulated emission cross sections, IEEE J. Quantum Electron. 18 (1982) 925–930, https://doi.org/10.1109/JQE.1982.1071611.

[48] S.A. Payne, L.L. Chase, L.K. Smith, W.L. Kway, W.F. Wyers, Infrared cross-section measurements for crystals doped with Er^{3+}, Tm^{3+}, and Ho^{3+}, IEEE J. Quantum Electron. 28 (1992) 2619–2630, https://doi.org/10.1109/3.161321.

[49] C. Sun, F. Yang, T. Cao, Z. You, Y. Wang, J. Li, Z. Zhu, C. Tu, Infrared spectroscopic properties of Tm^{3+}, Ho^{3+}:$NaY(WO_4)_2$ single crystals, J. Alloy. Compd. 509 (2011) 6987–6993, https://doi.org/10.1016/J.JALLCOM.2011.03.143.

[50] B.M. Walsh, N.P. Barnes, B.Di Bartolo, The temperature dependence of energy transfer between the Tm $^3F_4$ and Ho $^5I_7$ manifolds of Tm-sensitized Ho luminescence in YAG and YLF, J. Lumin. 90 (2000) 39–48, https://doi.org/10.1016/S0022-2313(99)00604-3.

[51] L.D. Merkle, J.B. Gruber, M.D. Seltzer, S.B. Stevens, T.H. Allik, Spectroscopic analysis of Tm^{3+}:$NaLa(MoO_4)_2$, J. Appl. Phys. 72 (1992) 4269–4274, https://doi.org/10.1063/1.352215.

[52] E.E. Dunaeva, L.I. Ivleva, M.E. Doroshenko, P.G. Zverev, A.V. Nekhoroshikh, V. V. Osiko, Synthesis, characterization, spectroscopy, and laser operation of $SrMoO_4$ crystals co-doped with Tm^{3+} and Ho^{3+}, J. Cryst. Growth 432 (2015) 1–5, https://doi.org/10.1016/J.JCRYSGRO.2015.09.006.